

1 Concurrent photochemical whitening and darkening of ambient 2 brown carbon

3 Qian Li¹, Dantong Liu^{1*}, Xiaotong Jiang¹, Ping Tian², Yangzhou Wu¹, Siyuan Li¹, Kang Hu¹, Quan Liu³,
4 Mengyu Huang², Ruijie Li², Kai Bi², Shaofei Kong⁴, Deping Ding²

5 ¹Department of Atmospheric Science, School of Earth Science, Zhejiang University, Hangzhou, 310027, China

6 ²Beijing Key Laboratory of Cloud, Precipitation and Atmospheric Water Resources, Beijing Meteorological Service, Beijing,
7 100089, China.

8 ³State Key Laboratory of Severe Weather & Key Laboratory of Atmospheric Chemistry of CMA, Chinese Academy of
9 Meteorological Sciences, Beijing, 100081, China

10 ⁴Department of Atmospheric Science, School of Environmental Science, China University of Geosciences, Wuhan, 430074,
11 China

12 *Correspondence to:* Dantong Liu (dantongliu@zju.edu.cn)

13 **Abstract.** The light-absorbing organic aerosol (OA), known as brown carbon (BrC), has important radiative impacts, however
14 its sources and evolution after emission remain to be elucidated. In this study, the light absorption at multiple wavelengths,
15 mass spectra of OA and microphysical properties of black carbon (BC) were characterized at a typical sub-urban environment
16 in Beijing. The absorption of BC is constrained by its size distribution and mixing state and the BrC absorption is obtained by
17 subtracting the BC absorption from the total aerosol absorption. Aerosol absorption was further apportioned to BC, primary
18 BrC and secondary BrC by applying the least-correlation between secondary BrC and BC. The multi-linear regression analysis
19 on the factorized OA mass spectra indicated the OA from traffic and biomass burning emission contributed to primary BrC.
20 Importantly, the moderately oxygenated OA (O/C=0.62) was revealed to highly correlate with secondary BrC. These OA had
21 higher nitrogen content, in line with the nitrogen-containing functional groups detected by the Fourier transform infrared
22 spectrometer. The photochemical processes were found to result in reduced contribution of fraction of total absorbance of
23 primary BrC about 20% but enhanced contribution of secondary BrC by 30%, implying the concurrent whitening and
24 darkening of BrC. This provides field evidence that the photochemically produced secondary nitrogen-containing OA can
25 considerably compensate some bleaching effect on the primary BrC, hereby causing radiative impacts.

26 1. Introduction

27 Atmospheric absorbing organic aerosol (OA), known as brown carbon (BrC), is an important contributor to anthropogenic
28 absorption besides black carbon (BC) (Laskin et al., 2015; Liu et al., 2020), particularly at shorter visible wavelengths (Bahadur
29 et al., 2012). Due to complex compositions of OA, the primary sources and subsequent evolution of BrC in the atmosphere
30 remains to be explicitly understood and causes uncertainties in evaluating the radiative impacts of BrC (Liu et al., 2020).

31 The chromophores of BrC are mainly aromatic compounds associated with certain functional groups (Liu et al., 2015c).
32 Particularly, compounds containing nitro, nitrated or other forms of nitrogen-containing functional groups are more absorbing
33 (Nakayama et al., 2013; Jacobson, 1999). It is well established that primary OA, especially from biomass burning, contains a
34 large fraction of BrC (Andreae and Crutzen, 1997; Rizzo et al., 2013; Bond, 2001). These primary BrC has a range of
35 absorptivity, which was found to be controlled by burning phases. OA co-emitting with BC (the flaming phase) exhibited a
36 higher absorptivity than OA-dominated smoldering phase (Liu et al., 2021). BrC can experience reactions with atmospheric
37 oxidants after emission. Previous studies (Satish et al., 2017; Satish and Rastogi, 2019; Dasari et al., 2019) found nitrogenous
38 compounds from biomass burning were responsible for BrC over South Asia and the chromophores were photobleached in the
39 afternoon. Numerous field and laboratory studies found the decrease of BrC absorptivity due to photobleaching of
40 chromophores, with lifetime ranging from a few hours (Zhao et al., 2015; Liu et al., 2021) to a few days (Forrister et al., 2015),
41 which may depend on the concentration of ambient hydroxyl radical (Wang et al., 2014), also influenced by relative humidity
42 and particle volatility (Schnitzler et al., 2020). The absorptivity of BrC could be also enhanced due to addition of functional
43 groups by forming conjugated structure with aromatics. This was supported by a number of laboratory studies that BrC
44 absorptivity could be enhanced when forming nitrogen-containing organic compounds, such as the formation of nitro-
45 aromatics when aromatics reacted with NO_x (Nakayama et al., 2013), or produced organic amine after reacting with ammonia
46 (Updyke et al., 2012). The enhancement of BrC absorptivity could occur either through nitration of existing chromophores, or
47 formation of new secondary organic aerosol (SOA) chromophores through gas-phase oxidation.

48 The above findings mean the enhancement or bleaching of BrC absorptivity via photooxidation will coexist. The time scale
49 between both competing processes will ultimately determine the lifetime of BrC in the atmosphere. However, both processes
50 have been rarely investigated in the field to explicitly determine the BrC components which principally determine the
51 respective enhancement or decrease of its absorptivity, particularly in regions influenced by combined anthropogenic sources.
52 In this study, by measurements using multiple-wavelength absorption and microphysical properties of BC in a sub-urban region,
53 the absorption of BC, primary and secondary BrC was discriminated. In conjunction with source attribution via OA mass
54 spectra, we are able to link the segregated absorption with certain sources and investigate their primary information and
55 subsequent evolution. The competition between photobleaching and secondary formation of BrC was investigated in real world.

56 2. Experimental and instrumentation

57 2.1 Site description and meteorology

58 The experiment was conducted during springtime at the Beijing Cloud Laboratory and Observational Utilities Deployment
59 Base (117.12°E, 40.14°N), which is located in the northeast suburban area in Beijing (Fig S1a). The site is surrounded by the
60 northwest mountain ridge, without significant local primary anthropogenic emissions (Hu et al., 2021). The 72-h backward
61 trajectories with every 3 hours initializing from the site are analyzed by the HYSPLIT model (Draxier and Hess, 1998) using
62 the 3-hourly 1°×1° meteorological field from the GDAS reanalysis product. The obtained backward trajectories were further
63 clustered to group the similar transport pathways (Makra et al., 2011). The meteorological parameters, including the
64 temperature (T), ambient relative humidity (RH), wind speed (WS) and wind direction (WD) were measured by a monitoring
65 station on the site.

66 2.2 Measurements of BC microphysics and absorption coefficient

67 In this study, the ambient aerosols were sampled by a large-flow (1.05 m³ min⁻¹) air particle sampler (TH-1000C II) with a
68 PM_{2.5} impactor (BGI SCC 1.829) and dried by a silica drier before measurement. The single particle soot photometer (SP2,
69 DMT., USA) used continuous laser at $\lambda=1064\text{nm}$ to incandescence light-absorbing aerosols (such as BC) for irradiating detectable
70 visible light. The incandescence signal was used to measure the refractory black carbon (rBC) mass. The SP2 incandescence
71 signal was calibrated using the Aquadag standard (Acheson Inc., USA), and a factor of 0.75 was applied to correct for ambient
72 BC (Laborde et al., 2012). The scattering signal was calibrated by monodispersed polystyrene latex spheres (PSL). The BC
73 core diameter (D_c) was calculated from the measured BC mass by assuming a BC density of 1.8 g cm⁻³ (Bond and Bergstrom,
74 2006). The leading edge only (LEO) method was applied to reconstruct the scattering signal of BC, which was used to
75 determine the coated particle diameter (D_p) by a Mie-lookup table with the inputs of scattering and incandescence signal of
76 each BC particle (Liu et al., 2014; Taylor et al., 2015). The mass median diameter (MMD) is derived from the D_c distribution,
77 which is determined as below and above MMD the rBC mass concentration is equal (Liu et al., 2019b). The bulk coating
78 thickness (D_p/D_c) is calculated as the cubic root of ratio of the total coated BC volume divided by the total volume of rBC.

79 The mass absorption cross section (MAC) (in m² g⁻¹) of each BC particle can be calculated using the measured coated and
80 uncoated BC sizes by applying the Mie core-shell calculation. The absorption coefficient of BC at certain wavelength, $\sigma_{\text{abs,BC}}$
81 (λ) is determined by multiplying the calculated MAC and rBC mass concentration at each size:

$$82 \sigma_{\text{abs,BC}}(\lambda) = \sum_i \text{MAC}(\lambda, D_{p,i}, D_{c,i}) m(\log D_{c,i}) \Delta \log D_{c,i} \quad (1)$$

83 where $m(\log D_{c,i})$ denotes the BC mass concentration at each logarithmic bin of D_c . The SP2 measurement at $\lambda=1064\text{nm}$ longer
84 than mostly populated BC size means the derived coatings and subsequent calculation of MAC is relatively independent of
85 particle shape within uncertainty of 21% (Liu et al., 2014; Hu et al., 2021).

86 The absorption coefficients at wavelengths $\lambda=375, 470, 528, 635$ and 880 nm were measured by a Micro-Aethalometer
87 (MA200, Aethlabs, San Francisco, CA, USA). Aerosol particles were collected on filter tapes, on which the light attenuation
88 was measured continuously with a time resolution of 30 s. The loading effect of filters was automatically corrected by

89 measuring attenuation at two different sampling flow rates on two spots in parallel (Drinovec et al., 2015a). Moreover, a multi-
90 scattering correction factor (C-value) of 3.5, 3.2 and 2.4 at the wavelengths 370 nm, 528 nm and 880 nm, respectively were
91 utilized to correct attenuation for the multiple light scattering effect. It was obtained by comparing the absorption coefficient
92 with a photoacoustic soot spectrometer (PASS-3, DMT) (Hu et al., 2021).

93 2.3 Attribution of primary and secondary BrC absorption coefficient

94 The absorption coefficient of BC at different λ is calculated using the measured uncoated core and coated size as mentioned
95 above. The absorption coefficient of total BrC is obtained by subtracting the BC absorption coefficient from the total absorption
96 at certain wavelength, expressed as:

$$97 \sigma_{\text{abs, BrC}}(\lambda) = \sigma_{\text{abs, total}}(\lambda) - \sigma_{\text{abs, BC}}(\lambda) \quad (2)$$

98 where the absorption coefficient of BC ($\sigma_{\text{abs, BC}}$) is obtained from the SP2 measurement, $\sigma_{\text{abs, total}}(\lambda)$ is the total light absorption
99 of aerosols measured by the MA200. The absorption coefficient of secondary BrC, the absorption not contributed by primary
100 sources, is obtained by subtracting the absorption of all primary sources from the total absorption (Crilley et al., 2015),
101 expressed as:

$$102 \sigma_{\text{abs, secBrC}}(\lambda) = \sigma_{\text{abs, total}}(\lambda) - \sigma_{\text{abs, pri}}(\lambda) \quad (3)$$

103 where $\sigma_{\text{abs, pri}}(\lambda)$ is the light absorption from primary sources. Here an assumption is made that light absorption from primary
104 aerosols is all from combustion sources, and these sources necessarily contain BC (Wang et al., 2018). Therefore, the total
105 absorption from primary sources can be obtained by scaling a factor from the mass concentration of BC, expressed as:

$$106 \sigma_{\text{abs, pri}}(\lambda) = \left(\frac{\sigma_{\text{abs, total}}}{[\text{rBC}]} \right)_{\text{pri}} \cdot [\text{rBC}]$$

107 (4)

108 where [rBC] is the mass concentration of rBC measured by the SP2, $\left(\frac{\sigma_{\text{abs, total}}}{[\text{rBC}]} \right)_{\text{pri}}$ is the scaling factor to derive the
109 absorption of primary combustion sources from [rBC]. This factor is obtained using the minimum R-squared (MRS) approach
110 (Wu and Yu, 2016), by adjusting the factor until a minimum correlation between $\sigma_{\text{abs, secBrC}}$ and [rBC] is reached because the
111 absorption from secondary sources are least likely to covary with that from primary sources (Wang et al., 2019a). This method
112 has been used in urban and sub-urban environment to obtain the primary BrC associated with combustion sources. Being
113 different from previous studies, an auxiliary characterization of rBC mass measured by the SP2 is used here to avoid the
114 possible interference from absorption measured by the same instrument. The $\left(\frac{\sigma_{\text{abs, total}}}{[\text{rBC}]} \right)_{\text{pri}}$ ratio at $\lambda=375$ nm, 470 nm, 528
115 nm, 635 nm and 880 nm is calculated to be 20.7, 17.0, 14.4, 11.7 and 5, respectively (Fig. S2), which falls within the reported
116 values from previous studies 11-50 (Zhang et al., 2020; Wang et al., 2019a). This scenario assumes a relatively consistent
117 absorption relative to BC mass concentration from sources during experiment. This however may not include some sporadic
118 events when sources with distinct OA or BC mass fraction may be introduced and alter the single $\left(\frac{\sigma_{\text{abs, total}}}{[\text{rBC}]} \right)_{\text{pri}}$ ratio. The

119 $\sigma_{\text{abs,secBrC}}$ therefore represents the overall mean value during the experimental period but this ratio will vary with seasons and
120 locations. The σ_{abs} of primary BrC can then be calculated as:

$$121 \sigma_{\text{abs,priBrC}}(\lambda) = \sigma_{\text{abs,BrC}}(\lambda) - \sigma_{\text{abs,secBrC}}(\lambda) \quad (5)$$

122 where $\sigma_{\text{abs,BrC}}$ and $\sigma_{\text{abs,secBrC}}$ is calculated from Equation (2) and (3), respectively.

123 2.4 Composition measurement

124 The mass concentration and chemical composition of non-refractory sub-micron PM (NR-PM₁) including organic aerosols
125 (OA), nitrate (NO₃⁻), sulfate (SO₄²⁻), chloride (Cl⁻) and ammonium (NH₄⁺) were determined with a High-Resolution Time-of-
126 Flight Aerosol Mass Spectrometer (HR-ToF-AMS, Aerodyne Research Inc., USA). The setup, operation, and calibration
127 procedures of the AMS have been described elsewhere (Canagaratna et al., 2007). During this field observation, the AMS was
128 operated in V-mode for the quantification of mass concentrations. The composition-dependent collection efficiencies were
129 applied (Middlebrook et al., 2012), and the ionization efficiency was calibrated using 300 nm pure ammonium nitrate (Jayne
130 et al., 2000). Elemental ratios of OA including oxygen-to-carbon (O/C), hydrogen-to-carbon (H/C) and nitrogen-to-carbon
131 (N/C) were determined to the improved-ambient method (Canagaratna et al., 2015).

132 Positive Matrix Factorization (PMF) (Paatero and Tapper, 1994) was performed on the inorganic and organic high-resolution
133 mass spectra to distinguish OA components from different sources (Zhang et al., 2011; Ulbrich et al., 2009; Decarlo et al.,
134 2010). The mass spectra of the combined matrix for m/z < 120 were excluded in PMF analysis. Five OA factors were identified.
135 The diagnostics of PMF is summarized in Text S1 and Fig. S6.

136 2.5 Offline Fourier transform infrared spectrometer (FTIR) analysis

137 Particulate Matter (PM) samples were collected once a day onto prebaked (600°C, 4h) quartz fiber filters (Whatman, QMA,
138 USA) using a large-flow (1.05 m³ min⁻¹) air particle sampler (TH-1000C II). The collected filter samples were stored in the
139 refrigerator at -20°C before analysis. The infrared spectra of collected samples were measured by a Fourier transform infrared
140 spectrometer (FTIR, Thermo Scientific, USA) equipped with an iD5 attenuated total reflectance accessory (diamond crystal)
141 to quantify the chemical functional groups over the wavenumbers range of 550-4000 cm⁻¹ with a resolution of 0.5 cm⁻¹. The
142 NO and NO₂ symmetric stretch in the FTIR spectra can characterize the functional groups associated with nitrogen-containing
143 organics (Coury and Dillner, 2008). Fig. S3 shows typical examples of FTIR spectra and the assigned functional groups for
144 the three pollution levels during experiment. The peak at 1110 cm⁻¹ corresponds to the background of the quartz fiber filter
145 overlapped with some X-H bending vibrations, which is subtracted for the following analysis. The characteristic organic nitrate
146 spectra appear at wavenumbers 860 cm⁻¹ (NO symmetric stretch), 1280 cm⁻¹ (NO₂ symmetric stretch) and 1630-1640 cm⁻¹
147 (NO₂ asymmetric stretch) (Bruns et al., 2010). After baseline calibration, The FTIR peaks of 1630 cm⁻¹ and 860 cm⁻¹ are
148 integrated the absorption areas above the baseline. The summed integrated area of -NO and -NO₂ are hereby used to indicate
149 the nitrogen-containing organics. There was no discernable peak of carbonyl group for our infrared spectrum, and the peak of

150 OH at 2500 cm^{-1} - 3400 cm^{-1} for the carboxylic acid is not discernable neither, thus the influence of ketone and carboxylic acid
151 may be of less importance for our dataset.

152 3. Results and Discussion

153 3.1 Source attributed OA

154 The overview results are shown in Fig. S1. The organics dominated the aerosol compositions for most time, but occasionally
155 nitrate was the most abundant component (Fig. S1g). Note that the nitrate here may also include components containing in
156 organics besides ammonium nitrate. Backward trajectories (Fig. S1a-d) showed that the most abundant PM_{10} concentration was
157 associated with air masses transported in shorter distance from southern regions (C1), but the longer and faster northerly
158 transported air mass from cleaner north (C2) could dilute the concentrations.

159 The resolved OA factors by the PMF analysis are shown in Fig. 1, including the mass spectra, time series and diurnal profiles
160 of each PMF factor with corresponded external and internal tracers. Three primary OA (POA) were identified as hydrocarbon-
161 like OA (HOA), cooking-related OA (COA), biomass burning OA (BBOA), with O/C of 0.31, 0.18 and 0.39 respectively.
162 These POA had considerable fraction of hydrocarbon fragments (C_xH_y), indicating their less aged status. The HOA profile was
163 characterized by higher contributions of aliphatic hydrocarbons and has dominated ion tracers such as m/z 41 (C_3H_5^+), 43
164 (C_3H_7^+), 55 (C_4H_7^+) and 57 (C_4H_9^+). The HOA concentration correlated with BC ($r=0.62$), which emits from traffic emissions.
165 The diurnal variation exhibited strong morning and afternoon rush-hour peaks of mass concentration. This factor was consistent
166 with the mass spectra of previously measured HOA from on-road vehicle emissions in urban cities (Zhang et al., 2005; Aiken
167 et al., 2009; Sun et al., 2016; Hu et al., 2017), which has m/z peaks characteristic of hydrocarbon fragments in series of $\text{C}_n\text{H}_{2n+1}^+$
168 and $\text{C}_n\text{H}_{2n-1}^+$. The mass spectrum of HOA shows overall similarity to those of primary OA emitted from gasoline and diesel
169 combustion sources ($r=0.68$) (Elser et al., 2016).

170 The OA from cooking sources (COA) is also characterized by prominent hydrocarbon ion series, however, with higher signal
171 at $\text{C}_n\text{H}_{2n-1}^+$ than $\text{C}_n\text{H}_{2n+1}^+$. COA had apparent fragments of both C_4H_9^+ and $\text{C}_3\text{H}_3\text{O}^+$, and has a higher ratio of $\text{C}_3\text{H}_3\text{O}^+/\text{C}_3\text{H}_5\text{O}^+$
172 (3.1), $\text{C}_4\text{H}_7^+/\text{C}_4\text{H}_9^+$ (2.2) than HOA (0.9–1.1), with cooking-related fragments of $\text{C}_5\text{H}_8\text{O}^+$ (m/z 84), $\text{C}_6\text{H}_{10}\text{O}^+$ (m/z 98) and
173 $\text{C}_7\text{H}_{12}\text{O}^+$ (m/z 112) (Sun et al., 2011b; Mohr et al., 2012). The COA shows overall similar spectral pattern to the reference
174 spectra of COA ($r=0.92$) (Elser et al., 2016). Its minor peak at noon and larger peak in the evening (Fig. 11) also corresponded
175 with the lunch and dinner time respectively. There was only a minor peak at noon for COA, which may be due to the sub-urban
176 nature of the site where the major aerosols from cooking sources may have been processed and lost the signature near source.
177 The feature of this factor was also observed in sub-urban environment (Huang et al., 2021).

178 The BBOA factor was identified based on the prominent signals of m/z 60 ($\text{C}_2\text{H}_4\text{O}_2^+$) and 73($\text{C}_3\text{H}_5\text{O}_2^+$), which are known
179 fragments of levoglucosan (Cubison et al., 2011). And BBOA also correlated with potassium (K^+ , $r = 0.80$), which are indicator
180 of biomass burning (Pachon et al., 2013; Brown et al., 2016). The m/z 60 and 73 together with a unique diurnal variation have

181 been shown to be a robust marker for the presence of aerosols from biomass burning emissions in many urban locations (Sun
182 et al., 2016). The BBOA shows very similar mass spectral patterns to previously reported reference spectra of biomass burning
183 ($r=0.94$) (Elser et al., 2016). The BBOA factor that was identified in spring accounted for 12.8% of the total OA in Beijing,
184 similar to previous reports (Hu et al., 2017). Biomass (Cheng et al., 2013) and solid fuel burning emissions (Sun et al., 2014)
185 have been widely observed to importantly contribute to the primary OA in this region. This off-road combustion source was
186 particularly abundant during wintertime for residential heating activities (Shen et al., 2019; Yang et al., 2018; Liu et al., 2016),
187 while boiler for industry use (mostly using coal as fuel) was in operation throughout the year (Liu et al., 2015b). During the
188 springtime of the experiment, the residential heating activities dropped due to increased ambient temperature thus the BBOA
189 may be mainly contributed by the industry sector.

190 Two types of oxygenated organic aerosols (OOA) were identified, in moderate (OOA2, $O/C=0.62$) and high oxidation state
191 (OOA1, $O/C=0.95$), respectively, which is very similar to the spectra of OOA factors resolved in other cities (Hayes et al.,
192 2013; Ulbrich et al., 2009). The average mass spectrum of OOA2 in this study is characterized by m/z 29 (mainly CHO^+), 43
193 (mainly $\text{C}_2\text{H}_3\text{O}^+$) and m/z 44 (CO_2^+), similar to the semi-volatile OOA spectrum identified in other locations (Sun et al., 2011a;
194 Zhou et al., 2016). On average, OOA2 accounts for 42% and 18% of $\text{C}_x\text{H}_y\text{O}^+$ and $\text{C}_x\text{H}_y\text{O}_2^+$ ions, respectively (Fig. 1b). These
195 results clearly indicate that OOA2 was primarily composed of less oxygenated, possibly freshly oxidized organics. Notably,
196 OOA2 had a substantially higher N/C than other factors ($N/C=0.037$), and had highest correlation with nitrate ($r=0.77$) and
197 with $\text{C}_x\text{H}_y\text{N}_z$ and $\text{C}_x\text{H}_y\text{N}_z\text{O}_p$ fragments ($r=0.83$). This factor therefore tends to largely result from nitrogen-containing OA and
198 its elevation at night may be also associated with dark oxidation by nitrate radical.

199 The mass spectrum of OOA1, which was characterized by a dominant peak at m/z 44 (mainly CO_2^+), a highest O/C (0.95). On
200 average, OOA1 contributes 51% of the $\text{C}_x\text{H}_y\text{O}^+$ signal and 23% of the $\text{C}_x\text{H}_y\text{O}_2^+$ signal (Fig. 1a). OOA1 showed particularly
201 high correlation with sulfate ($r=0.40$) because of their similar volatilities (Huffman et al., 2009; Jimenez et al., 2009). The
202 slight enhancement at noon for OOA1 (also for OOA2) soon after morning rush-hour indicated the likely rapid formation of
203 SOA through photooxidation. This significantly higher mean OOA2 than median value in the diurnal pattern indicated that
204 this OA type was largely associated with pollution events. Both OOA1 and OOA2 showed nighttime peak maybe due to
205 reduced boundary layer.

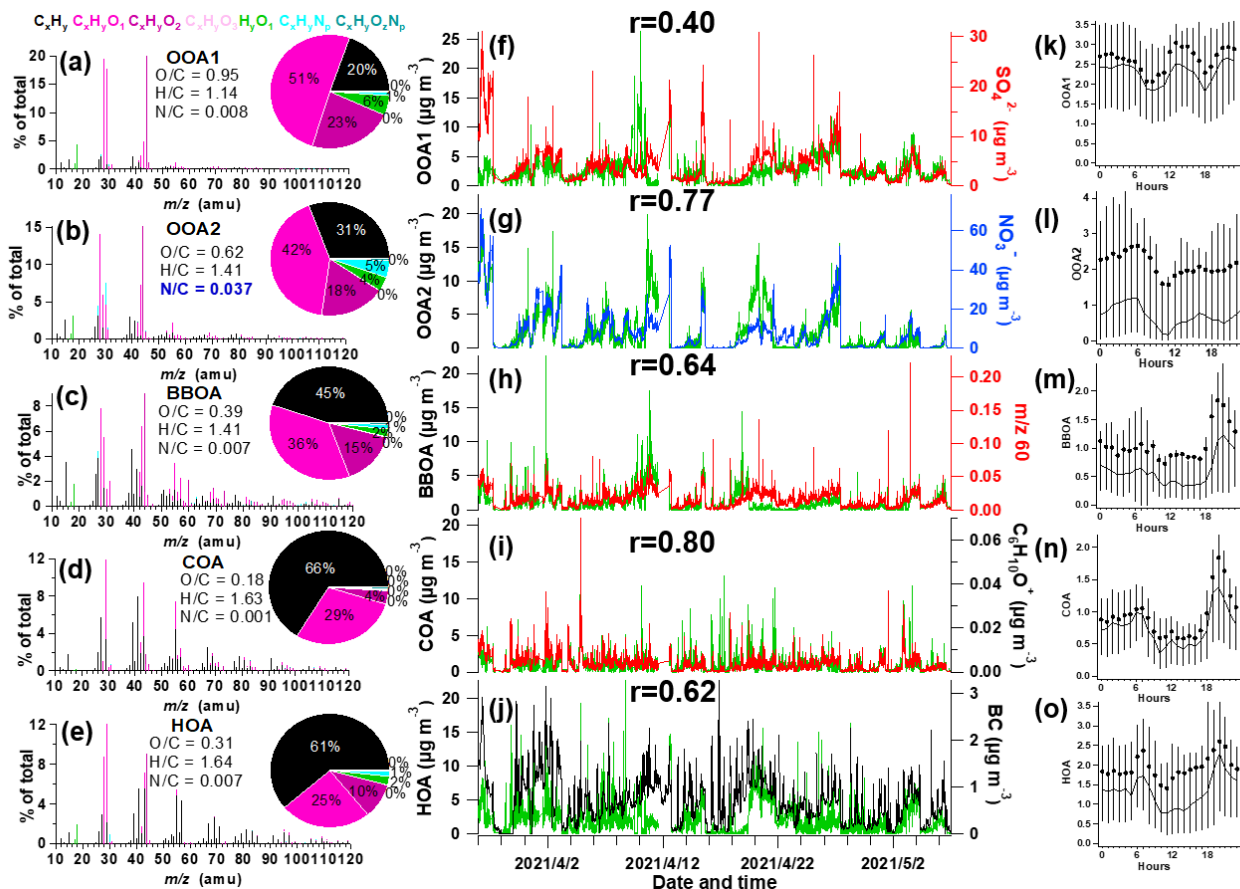
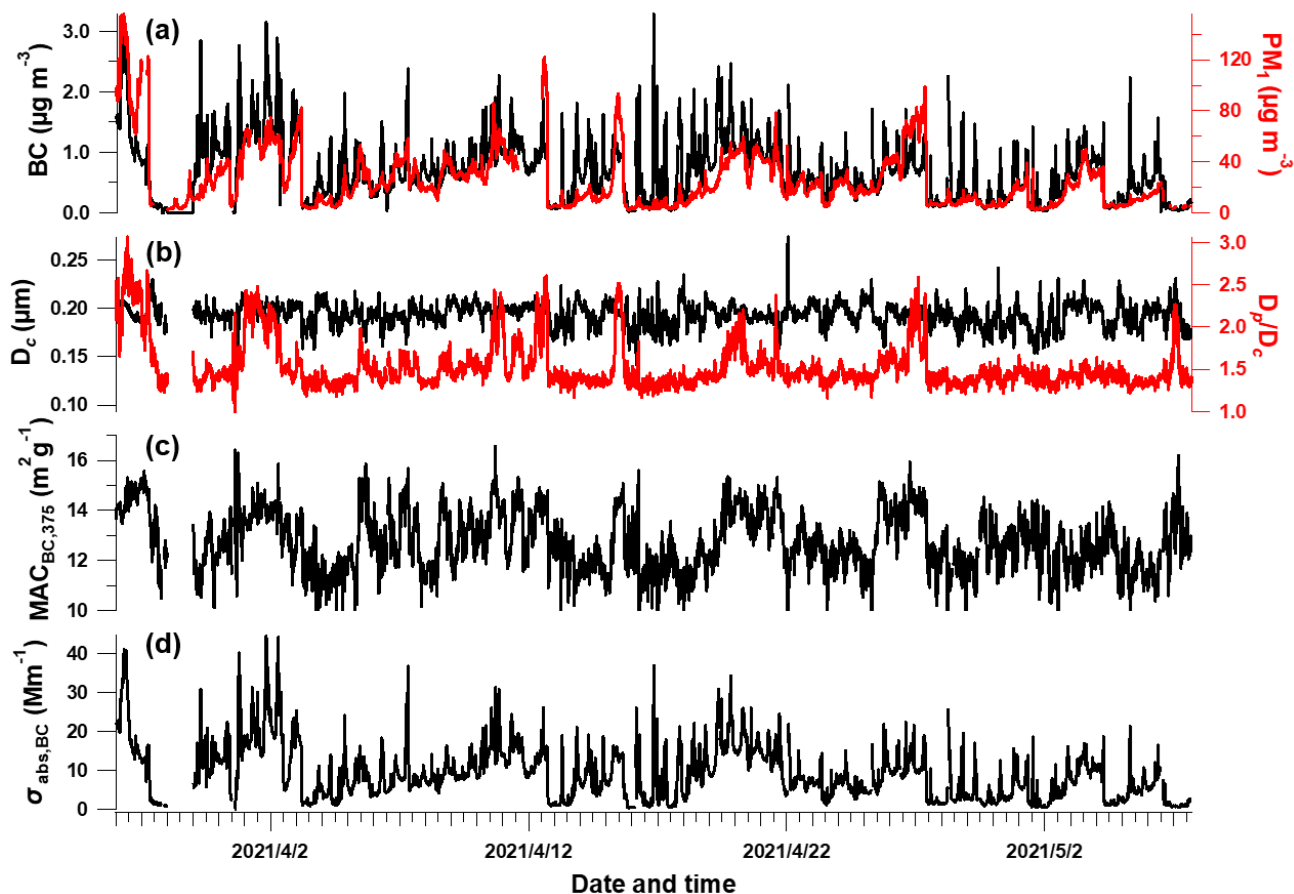


Figure 1. Information of source-apportioned organic aerosols by the PMF analysis. Mass spectra of (a) oxygenated OA1 (OOA1), (b) oxygenated OA2 (OOA2), (c) biomass burning OA (BBOA), (d) cooking-related OA (COA), (e) hydrocarbon-like OA (HOA), (f-j) Temporal variations of each PMF factor and the corresponding marker species. (k-o) Diurnal profiles of each factor. The lines, dots and whiskers denote the median, mean and the 25th/75th percentiles at each hour respectively.

3.2 Segregated aerosol absorption

Fig. 2 shows the time series of BC properties, including the BC mass concentration, D_p/D_c , D_c , MAC and light absorption coefficient of BC (section 2.2). The MMD of BC core varied between 93 – 274 nm which may correspond to the source-specific information (Liu et al., 2019a) or coagulation process during ageing. The coating of BC (indicated by D_p/D_c) showed sporadic enhancement which was closely associated with enhanced PM concentration (Fig. 2a). This was consistent with previous studies that high coatings of BC occurred during heavier pollution due to the enhanced secondary formation of condensable materials to particle phase (Ding et al., 2019; Zhang et al., 2018). This clearly indicates the variation of mixing state of BC and this will potentially influence its MAC and absorption Ångström exponent (AAE) (Liu et al., 2015a). It will introduce considerable uncertainties to use constant MAC or AAE to derive the absorption coefficient of BC at multiple wavelengths. The MAC estimated using the measured BC core size and coatings (Fig. 2c) is thus used to derive the $\sigma_{\text{abs,BC}}$ (section 2.2, shown in Fig. 2d). The $\sigma_{\text{abs,BC}}$ was $9.1 \pm 7.3 \text{ Mm}^{-1}$ during experimental period. MAC of BC at $\lambda=375\text{nm}$ showed to

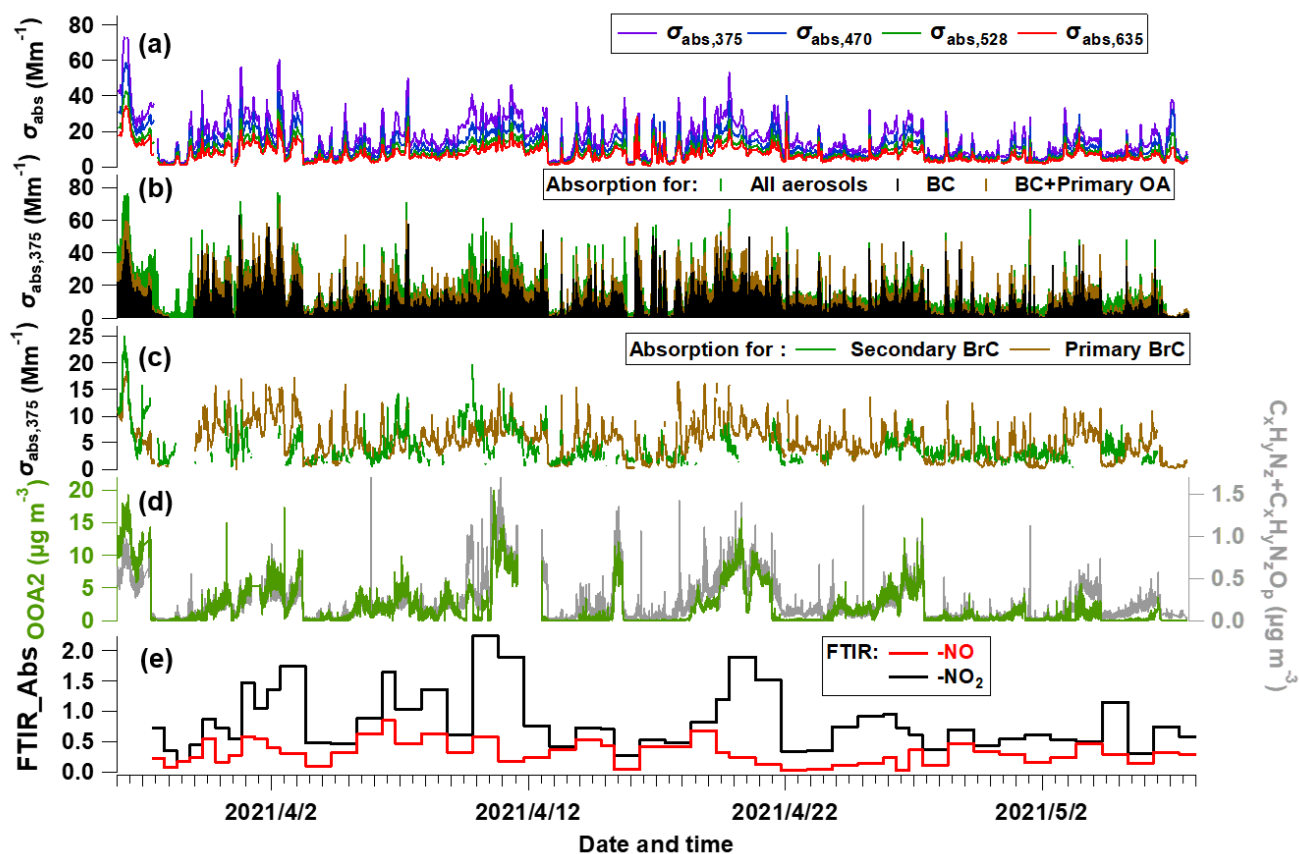
222 be at $8.4 - 16.6 \text{ m}^2 \text{ g}^{-1}$ with enhanced absorption when high coatings, which was consistent with previous studies which reported
 223 MACBC of $8-10 \text{ m}^2 \text{ g}^{-1}$, and higher value of $9.7 - 17.2 \text{ m}^2 \text{ g}^{-1}$ under polluted condition (Ding et al., 2019; Hu et al., 2021). The
 224 uncertainty of $\left(\frac{\sigma_{abs,total}}{[\text{rBC}]_{pri}}\right)$ is 4% for the data points over 1.5 according to (Wang et al., 2019a). The measurement of rBC
 225 mass from the SP2 had uncertainty of 20% (Schwarz et al., 2008), with relative coating thickness having uncertainty of 23%
 226 (Taylor et al., 2015), hereby resulting in a uncertainty of 27% for calculated MAC_{BC} . The above results in uncertainties of 31%
 227 and 20% for $\sigma_{\text{abs,BC}}$ and $\sigma_{\text{abs,pri}}$ respectively. The absorption measurement by MA200 had uncertainty of 25% (Drinovec et al.,
 228 2015b; Duesing et al., 2019). All these uncertainties propagates the uncertainties of $\sigma_{\text{abs,BrC}}$, $\sigma_{\text{abs,priBrC}}$ and $\sigma_{\text{abs,secBrC}}$ as 40%, 37%
 229 and 32% respectively. These are summarized in Table S1.



230
 231 **Figure 2. Temporal evolution of BC-related properties. (a) rBC and PM_{10} mass concentration, (b) BC core diameter and bulk coating**
 232 **thickness (D_p/D_c), (c) calculated mass absorption cross section (MAC) at $\lambda=375\text{nm}$, (d) absorption coefficient of BC.**

233 Using the method above, the total ($\sigma_{\text{abs,total}}$) and attributed absorption of BC ($\sigma_{\text{abs,BC}}$), primary ($\sigma_{\text{abs,priBrC}}$) and secondary BrC
 234 ($\sigma_{\text{abs,secBrC}}$) at $\lambda=375\text{nm}$ are shown in Fig. 3a-c. In Fig. 3b, the brown and green shades above the adjacent tracer indicate the
 235 absorption coefficient of primary and secondary BrC, respectively. Fig. 3c shows that the absorption coefficient of primary

236 BrC was higher than secondary BrC for most time, but for certain periods they were equivalent or secondary BrC occasionally
 237 exceeds primary BrC. The mean contribution of absorption coefficient for BC, primary BrC and secondary BrC is 51%, 27%
 238 and 22% in this study. The tracers associated with nitrogen-containing organics, such as OOA2 (with highest N/C), $C_xH_yN_z$
 239 and $C_xH_yN_zO_p$ fragments, and the FTIR measured $-NO + -NO_2$, are also shown in Fig. 3d-e.



240
 241 **Figure 3. Temporal evolution of segregated absorbing properties.** (a) Absorbing coefficients (σ_{abs}) at multiple wavelengths measured
 242 by the aethalometer, (b) σ_{abs} at $\lambda=375nm$ ($\sigma_{abs,375}$) for all aerosols, primary OA and BC, (c) $\sigma_{abs,375}$ for primary BrC and secondary
 243 BrC. (d) mass concentration of OOA2 and the $C_xH_yN_z$ and $C_xH_yN_zO_p$ fragments measured by the AMS. (e) FTIR-measured
 244 absorption of $-NO$ and $-NO_2$ bonds.

245 3.3 Source attribution of BrC absorption

246 A multiple linear regression (MLR) analysis is performed to apportion the absorption coefficient of BrC with the PMF
 247 attributed OA factors, expressed as:

$$248 \sigma_{abs,BrC} = a_0 + a_1 \cdot [OOA1] + a_2 \cdot [OOA2] + a_3 \cdot [BBOA] + a_4 \cdot [COA] + a_5 \cdot [HOA] \quad (6)$$

249 where a_1 to a_5 represents the regression coefficients for each factor. The contribution of each source-specific OA factor to
 250 $\sigma_{abs,BrC}$ can be obtained. This analysis is performed for the total BrC, primary and secondary BrC respectively. The results are
 251 shown in Table 1. MLR on the total BrC shows **relatively higher correction** ($r > 0.4$) with the factors of HOA, BBOA and OOA2,

252 suggesting the potential importance of the primary biomass burning and traffic source along with OOA2 in governing
 253 absorption of BrC. MLR analysis on the primary BrC distinguishes its substantial correlation with BBOA ($r=0.40$) and HOA
 254 ($r=0.46$), while MRL on the secondary BrC has a high correlation with OOA2 only ($r=0.44$). The MRL analysis links the
 255 apportioned absorption of physical properties with source-attributed chemical compositions, therefore validating and
 256 identifying the sources of primary and secondary BrC.

257 **Table 1. Results of the multilinear regression analysis (MLR) between $\sigma_{\text{abs},375}$ and the five PMF-resolved OA factors, with $\sigma_{\text{abs},375}$ of**
 258 **total BrC, primary and secondary BrC as dependent, respectively. All regression coefficients have passed the significance test with**
 259 **$p < 0.01$. Partial correlations above 0.4 are marked in bold. Since negative values appear when the COA participates, which is thus**
 260 **not included in the final regression but the values using COA factor are shown in brackets.**

Dependent	$\sigma_{\text{abs,BrC}}$		$\sigma_{\text{abs,pri BrC}}$		$\sigma_{\text{abs,sec BrC}}$	
Model	Regression coefficient	Partial correlation	Regression coefficient	Partial correlation	Regression coefficient	Partial correlation
Constant	2.26		1.67		1.47 (1.52)	
OOA1	0.57	0.23	0.04	0.02	0.46(0.46)	0.24 (0.24)
OOA2	1.22	0.53	0.37	0.25	0.74 (0.74)	0.44 (0.44)
BBOA	2.59	0.46	1.22	0.40	1.14 (1.18)	0.29 (0.29)
COA	1.30	0.22	1.45	0.36	/ (-0.25)	/ (-0.05)
HOA	1.70	0.47	1.17	0.46	0.49 (0.52)	0.20 (0.21)
R ²	0.77		0.63		0.55 (0.55)	

261 Importantly, an oxygenated secondary OA factor (OOA2) is identified to significantly contribute to the secondary BrC. This
 262 OOA has a moderate O/C (0.62) and a highest N/C of 0.037 among all factors. The high N/C means this factor contains the
 263 most abundant nitrogen-containing fragments, implied as its high correlation with the $\text{C}_x\text{H}_y\text{N}_z$ and $\text{C}_x\text{H}_y\text{N}_z\text{O}_p$ fragments ($r=0.83$,
 264 Fig. 3d) and with the FTIR absorption for -NO₂ and -NO bonds ($r=0.69$, Fig. S4). The -NO bond is mostly related to the
 265 organic nitrates (RONO₂), and -NO₂ peak could result from both organic nitrates and nitro-organics (Bruns et al., 2010). There
 266 is no discernable peak for organic amines. These all consistently imply that the OOA2 factor contained substantial fraction of
 267 nitrogen-containing organics, and these compounds have contributed to the absorption of secondary BrC.

268 3.4 Simultaneous whitening and darkening process of BrC

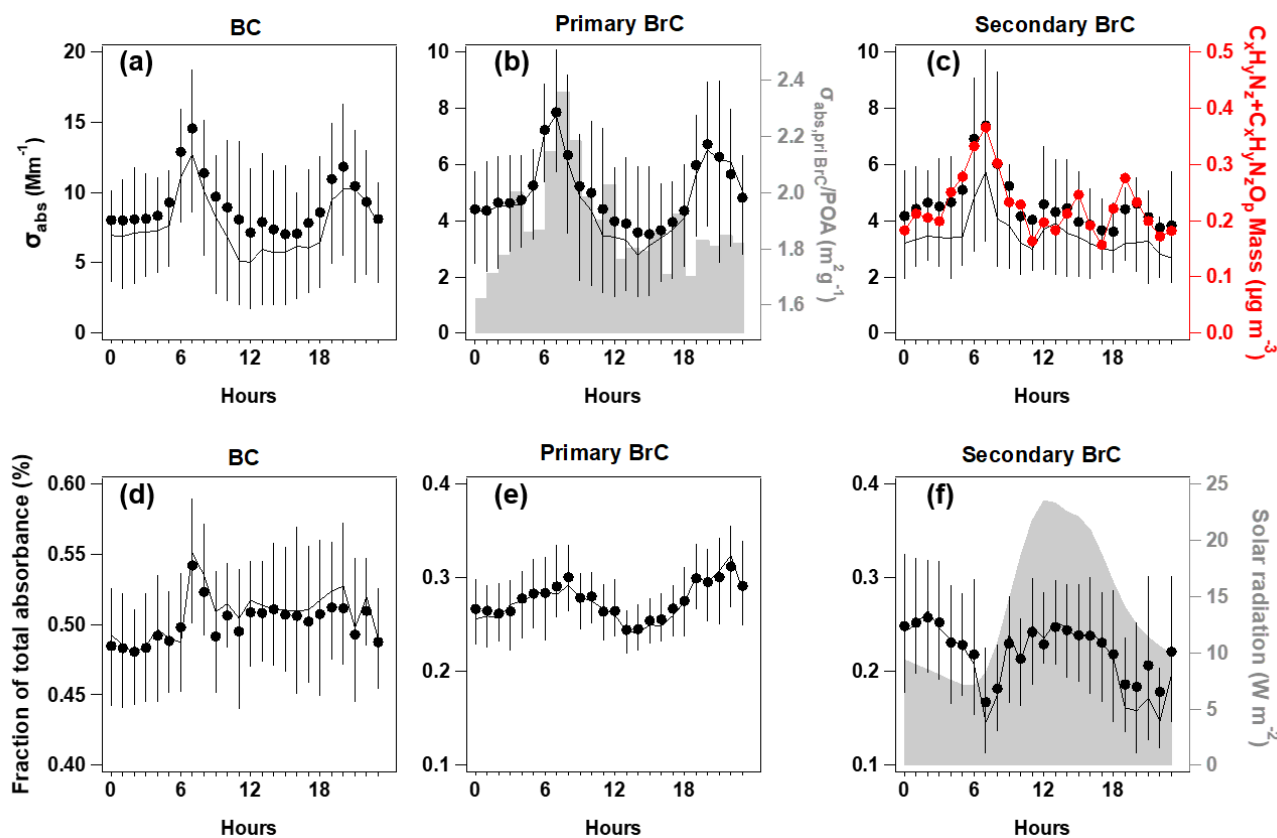
269 The relative contribution and diurnal variation of primary and secondary BrC measured by MA200 at 470, 528 and 635nm
 270 wavelengths are similar to those at 375nm wavelengths, but with decreased fraction of BrC absorption with increased
 271 wavelength. Due to the high contribution of BC to total absorption (>50% even at shortest wavelength), the spectral
 272 dependence of absorption in bulk has not shown apparent diurnal variation. The diurnal variation of $\sigma_{\text{abs},375}$ for BC and primary

273 BrC and their fractions showed consistent morning rush-hour peaks at 6:00-8:00 and the night-time enhancement due to
274 reduced boundary layer (Fig. 4a-b). This was in line with the morning peak of HOA and night peak of BBOA. The traffic
275 source in this region, in particular the diesel vehicles, was reported to emit considerable OA with certain chromophores, such
276 as aromatics (Yao et al., 2015) and heterocyclic organic compounds (Gentner et al., 2017; Schuetzle, 1983). In the morning
277 rush-hour, BC and primary BrC accounted for $51\pm 4\%$ and $29\pm 4\%$ in the total $\sigma_{\text{abs},375}$ respectively, with the remaining $20\pm 2\%$
278 classified as secondary BrC. The morning peak coinciding with the primary BrC may result from the rapid formation of BrC
279 from sources when emitted gases condensed and formed aerosols. These may lead to high cooccurrence between primary and
280 secondary BrC. Previous studies in urban environment also observed concurrent peaks of primary and secondary BrC, which
281 usually occurred at morning rush hour (Zhang et al., 2020). Furthermore, the assumption of the method used to apportion
282 primary and secondary BrC will cause some error in the distinction of absorption coefficient, it is possible that some of the
283 primary sources are being attributed to secondary sources and vice versa. This maybe a possible reason for the simultaneous
284 peak observed for primary and secondary BrC during morning rush hour. The night had contributions from BC and primary
285 BrC at $50\pm 2\%$ and $30\pm 3\%$ respectively, with $20\pm 3\%$ as secondary BrC. Fig. 4b showed the decrease of primary BrC absorption
286 tended to be more rapid than the HOA and BBOA mass (even a slight increase for HOA Fig. 1m and Fig. 1o), leading to
287 decreased absorption coefficient per unit mass of primary BrC (shade in Fig. 4b), which indicates the photobleaching process.
288 In addition to photobleaching, it possible that some primary species transformed into less absorbing secondary BrC species.
289 During this period, the type of HOA or BBOA that contribute to absorption may also have a lower absorptivity. In this context,
290 a recent chamber study reported that the primary BrC from biomass burning plumes could be bleached to half of the initial
291 absorptivity in 2-3 hours (Liu et al., 2021). Both HOA and BBOA had night peaks at 6-9pm with HOA having a higher
292 concentration than BBOA. The HOA/BBOA ratio almost unvaried in the diurnal pattern, thus had not resulted in a significant
293 variation of $\sigma_{\text{abs,priBrC}}/\text{POA}$ (Fig. 1m, Fig. 1o and Fig. 4b.).

294 Besides the morning rush-hour peak, there was an early afternoon peak for the absorption coefficient of secondary BrC,
295 prevailing the dilution effect of daytime boundary layer (Fig. 4c-S5). The night and morning peak of OOA2 and the morning
296 peak of $\sigma_{\text{abs,secBrC}}$ may result from primarily emitted moderately oxygenated OA, which was reported from some diesel sources
297 (Dewitt et al., 2015; Gentner et al., 2012). The fraction of secondary BrC thus had a pronounced early afternoon peak soon
298 after the peak solar radiation (Fig. 4f) and a peak after midnight soon after the nighttime peak of primary BrC (Fig. 4e). Fig
299 4e-f shows the photochemical processes led to an enhanced contribution of secondary BrC to the total absorption by 30% from
300 the morning rush-hour to midday, but during the same time reduced the contribution of primary BrC to the total absorption
301 about 20%. This shift of peaking time from primary to secondary BrC demonstrates the likely process of SOA formation from
302 gases, and these SOA compounds containing nitrogen (i.e., the OOA2) considerably contributed to the light absorption. This
303 ageing or oxidation likely occurred through photooxidation during early afternoon and aqueous processes (high RH conditions
304 prevail during nighttime) during nighttime. The oxidized volatile organic compounds (VOCs) with nitrogen chemistry involved
305 could condense to produce additional mass in particle phase (Ehn et al., 2014; Finewax et al., 2018). Due to the high NO_x
306 emission, photooxidation of traffic VOCs may have largely involved nitrogen chemistry. Previous studies found the NO_x -

307 involved SOA could produce considerable chromophores (Lin et al., 2015; Siemens et al., 2022), such as the traffic VOCs may
 308 produce SOA in a time scale of hours, containing nitro-aromatics (Wang et al., 2019b; Keyte et al., 2016). The daytime
 309 formation of organic nitrate may follow the gas-phase photooxidation mechanism, in which the excess NO could add to the
 310 peroxy radical to produce organic nitrate (Liebmann et al., 2019). The nighttime chemistry involving NO₃ radical through the
 311 oxidation of NO₂ by O₃, contributed to the important formation of organic nitrate by initializing the production of nitrooxy
 312 peroxy radicals (Ng et al., 2008; Rollins et al., 2012). Laboratory studies (Nakayama et al., 2013; Liu et al., 2015c) also widely
 313 observed the rapid production of nitrogen-containing OA involving NO_x chemistry could contribute to light absorption of
 314 aerosols.

315 Overall, by apportioning the absorption of primary and secondary BrC, we found the **photochemical processes** led to an
 316 enhanced contribution of **fraction of total absorbance of** secondary BrC by 30% but reduced contribution of primary BrC about
 317 20% in the semi-urban environment. This revealed that the whitening and darkening of BrC occurred simultaneously, and the
 318 secondary BrC produced by photooxidation may compensate some bleaching effect of primary BrC. The dominance of both
 319 competing processes may depend on the timescale and altitude in the atmosphere. For example, the enhanced BrC fraction
 320 observed above the planetary boundary layer may be explained by the enhanced secondary BrC (Tian et al., 2020), while
 321 further ageing may bleach the produced chromophores of these SOA.



322

323 **Figure 4. Diurnal variations of absorption coefficient at $\lambda=375\text{nm}$ ($\sigma_{\text{abs},375}$) for BC (a), primary BrC and absorption efficiency of**
324 **primary BrC ($\sigma_{\text{abs,priBrC}}$)/POA is shown in shade (b), and secondary BrC, along with the $\text{C}_x\text{H}_y\text{N}_z$ and $\text{C}_x\text{H}_y\text{N}_z\text{O}_p$ fragments (c); the**
325 **respective fraction in total for the segregated $\sigma_{\text{abs},375}$ (d-f), with direct radiation shown in shade. In each plot, the lines, dots and**
326 **whiskers denote the median, mean and the 25th/75th percentiles at each hour respectively.**

327 **4. Conclusion**

328 This study apportioned the shortwave absorption of BC, primary and secondary BrC, through concurrent measurements of BC
329 microphysical properties and OA mass spectra. The apportioned primary BrC absorption was linked with traffic and biomass
330 burning emissions, while secondary BrC was found to be associated with an oxygenated secondary OA factor with higher
331 nitrogen content. The enhancement of secondary BrC and decrease of primary BrC simultaneously occurred via daytime
332 photooxidation. The results emphasize the importance of nitrogen-containing OA in contributing to BrC. These OA could
333 primarily emit as aerosol phase, or in gas phase which requires further oxidation to be in aerosol phase to serve as BrC. The
334 NO_x -involved chemistry is prone to add nitrogen element to the existing OA and enhance the absorptivity of chromophores.
335 The anthropogenic NO_x emission could be therefore an important source in producing shortwave absorbing components in the
336 atmosphere, which may offset some of the conventionally-thought photobleaching of BrC.

337 **Acknowledgments**

338 This research was supported by the National Natural Science Foundation of China (Grant No. 42175116 and 41875167),
339 National Key R&D Program of China (2019YFC0214703).

340 **Author contribution**

341 D.L., X.J. and Qian L. prepared and designed the observation. D.L., Qian L., X.J and P.T. initiated the field campaign and
342 conducted the measurements. Qian L., D.L. P.T., Y.W., S.L. and K.H. contributed to the data analysis. Quan L., H.M., L.R.,
343 B.K., D.D. and S.K. provided technical support and assistance. Qian L. and D.L. wrote the manuscript. All authors read and
344 approved the final manuscript.

345

346 **References**

- 347 Aiken, A. C., Salcedo, D., Cubison, M. J., Huffman, J. A., DeCarlo, P. F., Ulbrich, I. M., Docherty, K. S., Sueper, D., Kimmel,
348 J. R., Worsnop, D. R., Trimborn, A., Northway, M., Stone, E. A., Schauer, J. J., Volkamer, R. M., Fortner, E., de Foy, B., Wang,
349 J., Laskin, A., Shutthanandan, V., Zheng, J., Zhang, R., Gaffney, J., Marley, N. A., Paredes-Miranda, G., Arnott, W. P., Molina,
350 L. T., Sosa, G., and Jimenez, J. L.: Mexico City aerosol analysis during MILAGRO using high resolution aerosol mass
351 spectrometry at the urban supersite (T0) - Part 1: Fine particle composition and organic source apportionment, *Atmos Chem*
352 *Phys*, 9, 6633-6653, 10.5194/acp-9-6633-2009, 2009.
- 353 Andreae, M. O. and Crutzen, P. J.: Atmospheric aerosols: Biogeochemical sources and role in atmospheric chemistry, *Science*,
354 276, 1052-1058, doi:10.1126/science.276.5315.1052, 1997.
- 355 Bahadur, R., Praveen, P. S., Xu, Y., and Ramanathan, V.: Solar absorption by elemental and brown carbon determined from
356 spectral observations, *Proceedings of the National Academy of Sciences of the United States of America*, 109, 17366-17371,
357 doi:10.1073/pnas.1205910109, 2012.
- 358 Bond, T. C.: Spectral dependence of visible light absorption by carbonaceous particles emitted from coal combustion,
359 *Geophysical Research Letters*, 28, 4075-4078, doi:10.1029/2001gl013652, 2001.
- 360 Bond, T. C. and Bergstrom, R. W.: Light absorption by carbonaceous particles: An investigative review, *Aerosol Science and*
361 *Technology*, 40, 27-67, doi:10.1080/02786820500421521, 2006.
- 362 Brown, S. G., Lee, T., Roberts, P. T., and Collett, J. L., Jr.: Wintertime Residential Biomass Burning in Las Vegas, Nevada;
363 Marker Components and Apportionment Methods, *Atmosphere*, 7, 10.3390/atmos7040058, 2016.
- 364 Bruns, E. A., Perraud, V., Zelenyuk, A., Ezell, M. J., Johnson, S. N., Yu, Y., Imre, D., Finlayson-Pitts, B. J., and Alexander, M.
365 L.: Comparison of FTIR and Particle Mass Spectrometry for the Measurement of Particulate Organic Nitrates, *Environmental*
366 *Science & Technology*, 44, 1056-1061, 10.1021/es9029864, 2010.
- 367 Canagaratna, M. R., Jimenez, J. L., Kroll, J. H., Chen, Q., Kessler, S. H., Massoli, P., Hildebrandt Ruiz, L., Fortner, E., Williams,
368 L. R., Wilson, K. R., Surratt, J. D., Donahue, N. M., Jayne, J. T., and Worsnop, D. R.: Elemental ratio measurements of organic
369 compounds using aerosol mass spectrometry: characterization, improved calibration, and implications, *Atmospheric Chemistry*
370 *and Physics*, 15, 253-272, doi:10.5194/acp-15-253-2015, 2015.
- 371 Canagaratna, M. R., Jayne, J. T., Jimenez, J. L., Allan, J. D., Alfarra, M. R., Zhang, Q., Onasch, T. B., Drewnick, F., Coe, H.,
372 Middlebrook, A., Delia, A., Williams, L. R., Trimborn, A. M., Northway, M. J., DeCarlo, P. F., Kolb, C. E., Davidovits, P., and
373 Worsnop, D. R.: Chemical and microphysical characterization of ambient aerosols with the aerodyne aerosol mass spectrometer,
374 *Mass Spectrometry Reviews*, 26, 185-222, doi:10.1002/mas.20115, 2007.
- 375 Cheng, Y., Engling, G., He, K. B., Duan, F. K., Ma, Y. L., Du, Z. Y., Liu, J. M., Zheng, M., and Weber, R. J.: Biomass burning
376 contribution to Beijing aerosol, *Atmospheric Chemistry and Physics*, 13, 7765-7781, doi:10.5194/acp-13-7765-2013, 2013.
- 377 Coury, C. and Dillner, A. M.: A method to quantify organic functional groups and inorganic compounds in ambient aerosols
378 using attenuated total reflectance FTIR spectroscopy and multivariate chemometric techniques, *Atmospheric Environment*, 42,

379 5923-5932, doi:10.1016/j.atmosenv.2008.03.026, 2008.

380 Crilley, L. R., Bloss, W. J., Yin, J., Beddows, D. C. S., Harrison, R. M., Allan, J. D., Young, D. E., Flynn, M., Williams, P.,
381 Zotter, P., Prevot, A. S. H., Heal, M. R., Barlow, J. F., Halios, C. H., Lee, J. D., Szidat, S., and Mohr, C.: Sources and
382 contributions of wood smoke during winter in London: assessing local and regional influences, *Atmos Chem Phys*, 15, 3149-
383 3171, 10.5194/acp-15-3149-2015, 2015.

384 Cubison, M. J., Ortega, A. M., Hayes, P. L., Farmer, D. K., Day, D., Lechner, M. J., Brune, W. H., Apel, E., Diskin, G. S.,
385 Fisher, J. A., Fuelberg, H. E., Hecobian, A., Knapp, D. J., Mikoviny, T., Riemer, D., Sachse, G. W., Sessions, W., Weber, R. J.,
386 Weinheimer, A. J., Wisthaler, A., and Jimenez, J. L.: Effects of aging on organic aerosol from open biomass burning smoke in
387 aircraft and laboratory studies, *Atmos Chem Phys*, 11, 12049-12064, 10.5194/acp-11-12049-2011, 2011.

388 Dasari, S., Andersson, A., Bikkina, S., Holmstrand, H., Budhavant, K., Satheesh, S., Asmi, E., Kesti, J., Backman, J., Salam,
389 A., Bisht, D. S., Tiwari, S., Hameed, Z., and Gustafsson, O.: Photochemical degradation affects the light absorption of water-
390 soluble brown carbon in the South Asian outflow, *Science Advances*, 5, 10.1126/sciadv.aau8066, 2019.

391 DeCarlo, P. F., Ulbrich, I. M., Crouse, J., de Foy, B., Dunlea, E. J., Aiken, A. C., Knapp, D., Weinheimer, A. J., Campos, T.,
392 Wennberg, P. O., and Jimenez, J. L.: Investigation of the sources and processing of organic aerosol over the Central Mexican
393 Plateau from aircraft measurements during MILAGRO, *Atmospheric Chemistry and Physics*, 10, 5257-5280, doi:10.5194/acp-
394 10-5257-2010, 2010.

395 DeWitt, H. L., Hellebust, S., Temime-Roussel, B., Ravier, S., Polo, L., Jacob, V., Buisson, C., Charron, A., Andre, M., Pasquier,
396 A., Besombes, J. L., Jaffrezo, J. L., Wortham, H., and Marchand, N.: Near-highway aerosol and gas-phase measurements in a
397 high-diesel environment, *Atmospheric Chemistry and Physics*, 15, 4373-4387, doi:10.5194/acp-15-4373-2015, 2015.

398 Ding, S., Liu, D., Zhao, D., Hu, K., Tian, P., Zhou, W., Huang, M., Yang, Y., Wang, F., Sheng, J., Liu, Q., Kong, S., Cui, P.,
399 Huang, Y., He, H., Coe, H., and Ding, D.: Size-Related Physical Properties of Black Carbon in the Lower Atmosphere over
400 Beijing and Europe, *Environmental Science & Technology*, 53, 11112-11121, doi:10.1021/acs.est.9b03722, 2019.

401 Draxier, R. R. and Hess, G. D.: An overview of the HYSPLIT_4 modelling system for trajectories, dispersion and deposition,
402 *Australian Meteorological Magazine*, 47, 295-308, 1998.

403 Drinovec, L., Mo?Nik, G., Zotter, P., Prév?t, A. S. H., Ruckstuhl, C., Coz, E., Rupakheti, M., Sciare, J., Müller, T., and
404 Wiedensohler, A.: The "dual-spot" Aethalometer: an improved measurement of aerosol black carbon with real-time loading
405 compensation, *Atmospheric Measurement Techniques*, 8, 1965-1979, 2015a.

406 Drinovec, L., Močnik, G., Zotter, P., Prévôt, A. S. H., Ruckstuhl, C., Coz, E., Rupakheti, M., Sciare, J., Müller, T., Wiedensohler,
407 A., and Hansen, A. D. A.: The "dual-spot" Aethalometer: an improved measurement of aerosol black carbon with real-time
408 loading compensation, *Atmos. Meas. Tech.*, 8, 1965-1979, 10.5194/amt-8-1965-2015, 2015b.

409 Duesing, S., Wehner, B., Mueller, T., Stoecker, A., and Wiedensohler, A.: The effect of rapid relative humidity changes on fast
410 filter-based aerosol-particle light-absorption measurements: uncertainties and correction schemes, *Atmospheric Measurement*
411 *Techniques*, 12, 5879-5895, 10.5194/amt-12-5879-2019, 2019.

412 Ehn, M., Thornton, J. A., Kleist, E., Sipila, M., Junninen, H., Pullinen, I., Springer, M., Rubach, F., Tillmann, R., Lee, B.,

413 Lopez-Hilfiker, F., Andres, S., Acir, I.-H., Rissanen, M., Jokinen, T., Schobesberger, S., Kangasluoma, J., Kontkanen, J.,
414 Nieminen, T., Kurten, T., Nielsen, L. B., Jorgensen, S., Kjaergaard, H. G., Canagaratna, M., Dal Maso, M., Berndt, T., Petaja,
415 T., Wahner, A., Kerminen, V.-M., Kulmala, M., Worsnop, D. R., Wildt, J., and Mentel, T. F.: A large source of low-volatility
416 secondary organic aerosol, *Nature*, 506, 476-+, doi:10.1038/nature13032, 2014.

417 Elser, M., Huang, R.-J., Wolf, R., Slowik, J. G., Wang, Q., Canonaco, F., Li, G., Bozzetti, C., Daellenbach, K. R., Huang, Y.,
418 Zhang, R., Li, Z., Cao, J., Baltensperger, U., El-Haddad, I., and Prevot, A. S. H.: New insights into PM_{2.5} chemical
419 composition and sources in two major cities in China during extreme haze events using aerosol mass spectrometry, *Atmos
420 Chem Phys*, 16, 3207-3225, 10.5194/acp-16-3207-2016, 2016.

421 Finewax, Z., de Gouw, J. A., and Ziemann, P. J.: Identification and Quantification of 4-Nitrocatechol Formed from OH and
422 NO₃ Radical-Initiated Reactions of Catechol in Air in the Presence of NO_x: Implications for Secondary Organic Aerosol
423 Formation from Biomass Burning, *Environmental Science & Technology*, 52, 1981-1989, doi:10.1021/acs.est.7b05864, 2018.

424 Forrister, H., Liu, J., Scheuer, E., Dibb, J., Ziemba, L., Thornhill, K. L., Anderson, B., Diskin, G., Perring, A. E., Schwarz, J.
425 P., Campuzano-Jost, P., Day, D. A., Palm, B. B., Jimenez, J. L., Nenes, A., and Weber, R. J.: Evolution of brown carbon in
426 wildfire plumes, *Geophysical Research Letters*, 42, 4623-4630, doi:10.1002/2015gl063897, 2015.

427 Gentner, D. R., Isaacman, G., Worton, D. R., Chan, A. W. H., Dallmann, T. R., Davis, L., Liu, S., Day, D. A., Russell, L. M.,
428 Wilson, K. R., Weber, R., Guha, A., Harley, R. A., and Goldstein, A. H.: Elucidating secondary organic aerosol from diesel and
429 gasoline vehicles through detailed characterization of organic carbon emissions, *Proceedings of the National Academy of
430 Sciences of the United States of America*, 109, 18318-18323, doi:10.1073/pnas.1212272109, 2012.

431 Gentner, D. R., Jathar, S. H., Gordon, T. D., Bahreini, R., Day, D. A., El Haddad, I., Hayes, P. L., Pieber, S. M., Platt, S. M.,
432 de Gouw, J., Goldstein, A. H., Harley, R. A., Jimenez, J. L., Prevot, A. S. H., and Robinson, A. L.: Review of Urban Secondary
433 Organic Aerosol Formation from Gasoline and Diesel Motor Vehicle Emissions, *Environmental Science & Technology*, 51,
434 1074-1093, doi:10.1021/acs.est.6b04509, 2017.

435 Hayes, P. L., Ortega, A. M., Cubison, M. J., Froyd, K. D., Zhao, Y., Cliff, S. S., Hu, W. W., Toohey, D. W., Flynn, J. H., Lefer,
436 B. L., Grossberg, N., Alvarez, S., Rappenglueck, B., Taylor, J. W., Allan, J. D., Holloway, J. S., Gilman, J. B., Kuster, W. C.,
437 De Gouw, J. A., Massoli, P., Zhang, X., Liu, J., Weber, R. J., Corrigan, A. L., Russell, L. M., Isaacman, G., Worton, D. R.,
438 Kreisberg, N. M., Goldstein, A. H., Thalman, R., Waxman, E. M., Volkamer, R., Lin, Y. H., Surratt, J. D., Kleindienst, T. E.,
439 Offenberg, J. H., Dusanter, S., Griffith, S., Stevens, P. S., Brioude, J., Angevine, W. M., and Jimenez, J. L.: Organic aerosol
440 composition and sources in Pasadena, California, during the 2010 CalNex campaign, *Journal of Geophysical Research-
441 Atmospheres*, 118, 9233-9257, 10.1002/jgrd.50530, 2013.

442 Hu, K., Liu, D., Tian, P., Wu, Y., Deng, Z., Wu, Y., Zhao, D., Li, R., Sheng, J., Huang, M., Ding, D., Li, W., Wang, Y., and Wu,
443 Y.: Measurements of the Diversity of Shape and Mixing State for Ambient Black Carbon Particles, *Geophysical Research
444 Letters*, 48, doi:10.1029/2021gl094522, 2021.

445 Hu, W., Hu, M., Hu, W.-W., Zheng, J., Chen, C., Wu, Y., and Guo, S.: Seasonal variations in high time-resolved chemical
446 compositions, sources, and evolution of atmospheric submicron aerosols in the megacity Beijing, *Atmos Chem Phys*, 17, 9979-

447 10000, 10.5194/acp-17-9979-2017, 2017.

448 Huang, D. D., Zhu, S., An, J., Wang, Q., Qiao, L., Zhou, M., He, X., Ma, Y., Sun, Y., Huang, C., Yu, J. Z., and Zhang, Q.:
449 Comparative Assessment of Cooking Emission Contributions to Urban Organic Aerosol Using Online Molecular Tracers and
450 Aerosol Mass Spectrometry Measurements, *Environmental Science & Technology*, 55, 14526-14535, 10.1021/acs.est.1c03280,
451 2021.

452 Huffman, J. A., Docherty, K. S., Aiken, A. C., Cubison, M. J., Ulbrich, I. M., DeCarlo, P. F., Sueper, D., Jayne, J. T., Worsnop,
453 D. R., Ziemann, P. J., and Jimenez, J. L.: Chemically-resolved aerosol volatility measurements from two megacity field studies,
454 *Atmospheric Chemistry and Physics*, 9, 7161-7182, doi:10.5194/acp-9-7161-2009, 2009.

455 Jacobson, M. Z.: Isolating nitrated and aromatic aerosols and nitrated aromatic gases as sources of ultraviolet light absorption,
456 *Journal of Geophysical Research-Atmospheres*, 104, 3527-3542, doi:10.1029/1998jd100054, 1999.

457 Jimenez, J. L., Canagaratna, M. R., Donahue, N. M., Prevot, A. S. H., Zhang, Q., Kroll, J. H., DeCarlo, P. F., Allan, J. D., Coe,
458 H., Ng, N. L., Aiken, A. C., Docherty, K. S., Ulbrich, I. M., Grieshop, A. P., Robinson, A. L., Duplissy, J., Smith, J. D., Wilson,
459 K. R., Lanz, V. A., Hueglin, C., Sun, Y. L., Tian, J., Laaksonen, A., Raatikainen, T., Rautiainen, J., Vaattovaara, P., Ehn, M.,
460 Kulmala, M., Tomlinson, J. M., Collins, D. R., Cubison, M. J., Dunlea, E. J., Huffman, J. A., Onasch, T. B., Alfarra, M. R.,
461 Williams, P. I., Bower, K., Kondo, Y., Schneider, J., Drewnick, F., Borrmann, S., Weimer, S., Demerjian, K., Salcedo, D.,
462 Cottrell, L., Griffin, R., Takami, A., Miyoshi, T., Hatakeyama, S., Shimono, A., Sun, J. Y., Zhang, Y. M., Dzepina, K., Kimmel,
463 J. R., Sueper, D., Jayne, J. T., Herndon, S. C., Trimborn, A. M., Williams, L. R., Wood, E. C., Middlebrook, A. M., Kolb, C.
464 E., Baltensperger, U., and Worsnop, D. R.: Evolution of Organic Aerosols in the Atmosphere, *Science*, 326, 1525-1529,
465 doi:10.1126/science.1180353, 2009.

466 Keyte, I. J., Albinet, A., and Harrison, R. M.: On-road traffic emissions of polycyclic aromatic hydrocarbons and their oxy-
467 and nitro-derivative compounds measured in road tunnel environments, *Science of the Total Environment*, 566, 1131-1142,
468 doi:10.1016/j.scitotenv.2016.05.152, 2016.

469 Laborde, M., Schnaiter, M., Linke, C., Saathoff, H., Naumann, K. H., Moehler, O., Berlenz, S., Wagner, U., Taylor, J. W., Liu,
470 D., Flynn, M., Allan, J. D., Coe, H., Heimerl, K., Dahlkoetter, F., Weinzierl, B., Wollny, A. G., Zannata, M., Cozic, J., Laj, P.,
471 Hitzenberger, R., Schwarz, J. P., and Gysel, M.: Single Particle Soot Photometer intercomparison at the AIDA chamber,
472 *Atmospheric Measurement Techniques*, 5, 3077-3097, doi:10.5194/amt-5-3077-2012, 2012.

473 Laskin, A., Laskin, J., and Nizkorodov, S. A.: Chemistry of Atmospheric Brown Carbon, *Chemical Reviews*, 115, 4335-4382,
474 doi:10.1021/cr5006167, 2015.

475 Liebmann, J., Sobanski, N., Schuladen, J., Karu, E., Hellen, H., Hakola, H., Zha, Q., Ehn, M., Riva, M., Heikkinen, L.,
476 Williams, J., Fischer, H., Lelieveld, J., and Crowley, J. N.: Alkyl nitrates in the boreal forest: formation via the NO₃-, OH- and
477 O-3-induced oxidation of biogenic volatile organic compounds and ambient lifetimes, *Atmospheric Chemistry and Physics*,
478 19, 10391-10403, doi:10.5194/acp-19-10391-2019, 2019.

479 Lin, P., Liu, J., Shilling, J. E., Kathmann, S. M., Laskin, J., and Laskin, A.: Molecular characterization of brown carbon (BrC)
480 chromophores in secondary organic aerosol generated from photo-oxidation of toluene, *Physical Chemistry Chemical Physics*,

481 17, 23312-23325, doi:10.1039/c5cp02563j, 2015.

482 Liu, D., He, C., Schwarz, J. P., and Wang, X.: Lifecycle of light-absorbing carbonaceous aerosols in the atmosphere, *npj*
483 *Climate and Atmospheric Science*, 3, 40, doi:10.1038/s41612-020-00145-8, 2020.

484 Liu, D., Taylor, J. W., Young, D. E., Flynn, M. J., Coe, H., and Allan, J. D.: The effect of complex black carbon microphysics
485 on the determination of the optical properties of brown carbon, *Geophysical Research Letters*, 42, 613-619,
486 doi:10.1002/2014gl062443, 2015a.

487 Liu, D., Allan, J. D., Young, D. E., Coe, H., Beddows, D., Fleming, Z. L., Flynn, M. J., Gallagher, M. W., Harrison, R. M., Lee,
488 J., Prevot, A. S. H., Taylor, J. W., Yin, J., Williams, P. I., and Zotter, P.: Size distribution, mixing state and source apportionment
489 of black carbon aerosol in London during wintertime, *Atmos Chem Phys*, 14, 10061-10084, 10.5194/acp-14-10061-2014, 2014.

490 Liu, D., Joshi, R., Wang, J., Yu, C., Allan, J. D., Coe, H., Flynn, M. J., Xie, C., Lee, J., Squires, F., Kotthaus, S., Grimmond,
491 S., Ge, X., Sun, Y., and Fu, P.: Contrasting physical properties of black carbon in urban Beijing between winter and summer,
492 *Atmos. Chem. Phys.*, 19, 6749-6769, doi:10.5194/acp-19-6749-2019, 2019a.

493 Liu, D., Joshi, R., Wang, J., Yu, C., Allan, J. D., Coe, H., Flynn, M. J., Xie, C., Lee, J., Squires, F., Kotthaus, S., Grimmond,
494 S., Ge, X., Sun, Y., and Fu, P.: Contrasting physical properties of black carbon in urban Beijing between winter and summer,
495 *Atmospheric Chemistry and Physics*, 19, 6749-6769, doi:10.5194/acp-19-6749-2019, 2019b.

496 Liu, D., Li, S., Hu, D., Kong, S., Cheng, Y., Wu, Y., Ding, S., Hu, K., Zheng, S., Yan, Q., Zheng, H., Zhao, D., Tian, P., Ye, J.,
497 Huang, M., and Ding, D.: Evolution of Aerosol Optical Properties from Wood Smoke in Real Atmosphere Influenced by
498 Burning Phase and Solar Radiation, *Environmental Science & Technology*, 55, 5677-5688, 10.1021/acs.est.0c07569, 2021.

499 Liu, F., Zhang, Q., Tong, D., Zheng, B., Li, M., Huo, H., and He, K. B.: High-resolution inventory of technologies, activities,
500 and emissions of coal-fired power plants in China from 1990 to 2010, *Atmospheric Chemistry and Physics*, 15, 13299-13317,
501 doi:10.5194/acp-15-13299-2015, 2015b.

502 Liu, J., Mauzerall, D. L., Chen, Q., Zhang, Q., Song, Y., Peng, W., Klimont, Z., Qiu, X., Zhang, S., Hu, M., Lin, W., Smith, K.
503 R., and Zhu, T.: Air pollutant emissions from Chinese households: A major and underappreciated ambient pollution source,
504 *Proceedings of the National Academy of Sciences of the United States of America*, 113, 7756-7761,
505 doi:10.1073/pnas.1604537113, 2016.

506 Liu, P. F., Abdelmalki, N., Hung, H. M., Wang, Y., Brune, W. H., and Martin, S. T.: Ultraviolet and visible complex refractive
507 indices of secondary organic material produced by photooxidation of the aromatic compounds toluene and m-xylene,
508 *Atmospheric Chemistry and Physics*, 15, 1435-1446, doi:10.5194/acp-15-1435-2015, 2015c.

509 Makra, L., Matyasovszky, I., Guba, Z., Karatzas, K., and Anttila, P.: Monitoring the long-range transport effects on urban
510 PM10 levels using 3D clusters of backward trajectories, *Atmospheric Environment*, 45, 2630-2641,
511 doi:10.1016/j.atmosenv.2011.02.068, 2011.

512 Mohr, C., DeCarlo, P. F., Heringa, M. F., Chirico, R., Slowik, J. G., Richter, R., Reche, C., Alastuey, A., Querol, X., Seco, R.,
513 Penuelas, J., Jimenez, J. L., Crippa, M., Zimmermann, R., Baltensperger, U., and Prevot, A. S. H.: Identification and
514 quantification of organic aerosol from cooking and other sources in Barcelona using aerosol mass spectrometer data,

515 Atmospheric Chemistry and Physics, 12, 1649-1665, doi:10.5194/acp-12-1649-2012, 2012.

516 Nakayama, T., Sato, K., Matsumi, Y., Imamura, T., Yamazaki, A., and Uchiyama, A.: Wavelength and NO_x dependent complex
517 refractive index of SOAs generated from the photooxidation of toluene, Atmospheric Chemistry and Physics, 13, 531-545,
518 doi:10.5194/acp-13-531-2013, 2013.

519 Ng, N. L., Kwan, A. J., Surratt, J. D., Chan, A. W. H., Chhabra, P. S., Sorooshian, A., Pye, H. O. T., Crounse, J. D., Wennberg,
520 P. O., Flagan, R. C., and Seinfeld, J. H.: Secondary organic aerosol (SOA) formation from reaction of isoprene with nitrate
521 radicals (NO₃), Atmospheric Chemistry and Physics, 8, 4117-4140, doi:10.5194/acp-8-4117-2008, 2008.

522 Paatero, P. and Tapper, U.: POSITIVE MATRIX FACTORIZATION - A NONNEGATIVE FACTOR MODEL WITH
523 OPTIMAL UTILIZATION OF ERROR-ESTIMATES OF DATA VALUES, Environmetrics, 5, 111-126,
524 doi:10.1002/env.3170050203, 1994.

525 Pachon, J. E., Weber, R. J., Zhang, X., Mulholland, J. A., and Russell, A. G.: Revising the use of potassium (K) in the source
526 apportionment of PM_{2.5}, Atmospheric Pollution Research, 4, 14-21, 10.5094/apr.2013.002, 2013.

527 Rizzo, L. V., Artaxo, P., Mueller, T., Wiedensohler, A., Paixao, M., Cirino, G. G., Arana, A., Swietlicki, E., Roldin, P., Fors, E.
528 O., Wiedemann, K. T., Leal, L. S. M., and Kulmala, M.: Long term measurements of aerosol optical properties at a primary
529 forest site in Amazonia, Atmospheric Chemistry and Physics, 13, 2391-2413, doi:10.5194/acp-13-2391-2013, 2013.

530 Rollins, A. W., Browne, E. C., Min, K. E., Pusede, S. E., Wooldridge, P. J., Gentner, D. R., Goldstein, A. H., Liu, S., Day, D.
531 A., Russell, L. M., and Cohen, R. C.: Evidence for NO_x Control over Nighttime SOA Formation, Science, 337, 1210-1212,
532 doi:10.1126/science.1221520, 2012.

533 Satish, R. and Rastogi, N.: On the Use of Brown Carbon Spectra as a Tool to Understand Their Broader Composition and
534 Characteristics: A Case Study from Crop-residue Burning Samples, Acs Omega, 4, 1847-1853, 10.1021/acsomega.8b02637,
535 2019.

536 Satish, R., Shamjad, P., Thamban, N., Tripathi, S., and Rastogi, N.: Temporal Characteristics of Brown Carbon over the Central
537 Indo-Gangetic Plain, Environmental Science & Technology, 51, 6765-6772, 10.1021/acs.est.7b00734, 2017.

538 Schnitzler, E. G., Liu, T., Hems, R. F., and Abbatt, J. P. D.: Emerging investigator series: heterogeneous OH oxidation of
539 primary brown carbon aerosol: effects of relative humidity and volatility, Environmental Science-Processes & Impacts, 22,
540 2162-2171, 10.1039/d0em00311e, 2020.

541 Schuetzle, D.: SAMPLING OF VEHICLE EMISSIONS FOR CHEMICAL-ANALYSIS AND BIOLOGICAL TESTING,
542 Environmental Health Perspectives, 47, 65-80, doi:10.2307/3429500, 1983.

543 Schwarz, J. P., Spackman, J. R., Fahey, D. W., Gao, R. S., Lohmann, U., Stier, P., Watts, L. A., Thomson, D. S., Lack, D. A.,
544 Pfister, L., Mahoney, M. J., Baumgardner, D., Wilson, J. C., and Reeves, J. M.: Coatings and their enhancement of black carbon
545 light absorption in the tropical atmosphere, Journal of Geophysical Research-Atmospheres, 113, 10.1029/2007jd009042, 2008.

546 Shen, G., Ru, M., Du, W., Zhu, X., Zhong, Q., Chen, Y., Shen, H., Yun, X., Meng, W., Liu, J., Cheng, H., Hu, J., Guan, D., and
547 Tao, S.: Impacts of air pollutants from rural Chinese households under the rapid residential energy transition, Nature
548 Communications, 10, doi:10.1038/s41467-019-11453-w, 2019.

549 Siemens, K., Morales, A., He, Q., Li, C., Hettiyadura, A. P. S., Rudich, Y., and Laskin, A.: Molecular Analysis of Secondary
550 Brown Carbon Produced from the Photooxidation of Naphthalene, *Environmental science & technology*, 56, 3340-3353,
551 doi:10.1021/acs.est.1c03135, 2022.

552 Sun, Y., Jiang, Q., Wang, Z., Fu, P., Li, J., Yang, T., and Yin, Y.: Investigation of the sources and evolution processes of severe
553 haze pollution in Beijing in January 2013, *Journal of Geophysical Research-Atmospheres*, 119, 4380-4398,
554 doi:10.1002/2014jd021641, 2014.

555 Sun, Y., Du, W., Fu, P., Wang, Q., Li, J., Ge, X., Zhang, Q., Zhu, C., Ren, L., Xu, W., Zhao, J., Han, T., Worsnop, D. R., and
556 Wang, Z.: Primary and secondary aerosols in Beijing in winter: sources, variations and processes, *Atmos Chem Phys*, 16, 8309-
557 8329, 10.5194/acp-16-8309-2016, 2016.

558 Sun, Y. L., Zhang, Q., Schwab, J. J., Chen, W. N., Bae, M. S., Lin, Y. C., Hung, H. M., and Demerjian, K. L.: A case study of
559 aerosol processing and evolution in summer in New York City, *Atmos Chem Phys*, 11, 12737-12750, 10.5194/acp-11-12737-
560 2011, 2011a.

561 Sun, Y. L., Zhang, Q., Schwab, J. J., Demerjian, K. L., Chen, W. N., Bae, M. S., Hung, H. M., Hogrefe, O., Frank, B., Rattigan,
562 O. V., and Lin, Y. C.: Characterization of the sources and processes of organic and inorganic aerosols in New York city with a
563 high-resolution time-of-flight aerosol mass spectrometer, *Atmospheric Chemistry and Physics*, 11, 1581-1602,
564 doi:10.5194/acp-11-1581-2011, 2011b.

565 Taylor, J. W., Allan, J. D., Liu, D., Flynn, M., Weber, R., Zhang, X., Lefer, B. L., Grossberg, N., Flynn, J., and Coe, H.:
566 Assessment of the sensitivity of core/shell parameters derived using the single-particle soot photometer to density and
567 refractive index, *Atmospheric Measurement Techniques*, 8, 1701-1718, doi:10.5194/amt-8-1701-2015, 2015.

568 Tian, P., Liu, D., Zhao, D., Yu, C., Liu, Q., Huang, M., Deng, Z., Ran, L., Wu, Y., Ding, S., Hu, K., Zhao, G., Zhao, C., and
569 Ding, D.: In situ vertical characteristics of optical properties and heating rates of aerosol over Beijing, *Atmospheric Chemistry
570 and Physics*, 20, 2603-2622, doi:10.5194/acp-20-2603-2020, 2020.

571 Ulbrich, I. M., Canagaratna, M. R., Zhang, Q., Worsnop, D. R., and Jimenez, J. L.: Interpretation of organic components from
572 Positive Matrix Factorization of aerosol mass spectrometric data, *Atmos Chem Phys*, 9, 2891-2918, 10.5194/acp-9-2891-2009,
573 2009.

574 Updyke, K. M., Nguyen, T. B., and Nizkorodov, S. A.: Formation of brown carbon via reactions of ammonia with secondary
575 organic aerosols from biogenic and anthropogenic precursors, *Atmospheric Environment*, 63, 22-31,
576 doi:10.1016/j.atmosenv.2012.09.012, 2012.

577 Wang, Q., Han, Y., Ye, J., Liu, S., Pongpiachan, S., Zhang, N., Han, Y., Tian, J., Wu, C., Long, X., Zhang, Q., Zhang, W., Zhao,
578 Z., and Cao, J.: High Contribution of Secondary Brown Carbon to Aerosol Light Absorption in the Southeastern Margin of
579 Tibetan Plateau, *Geophysical Research Letters*, 46, 4962-4970, 10.1029/2019gl082731, 2019a.

580 Wang, Q., Cao, J., Han, Y., Tian, J., Zhang, Y., Pongpiachan, S., Zhang, Y., Li, L., Niu, X., Shen, Z., Zhao, Z., Tipmanee, D.,
581 Bunsomboonsakul, S., Chen, Y., and Sun, J.: Enhanced light absorption due to the mixing state of black carbon in fresh biomass
582 burning emissions, *Atmospheric Environment*, 180, 184-191, doi:10.1016/j.atmosenv.2018.02.049, 2018.

583 Wang, X., Heald, C. L., Ridley, D. A., Schwarz, J. P., Spackman, J. R., Perring, A. E., Coe, H., Liu, D., and Clarke, A. D.:
584 Exploiting simultaneous observational constraints on mass and absorption to estimate the global direct radiative forcing of
585 black carbon and brown carbon, *Atmospheric Chemistry and Physics*, 14, 10989-11010, doi:10.5194/acp-14-10989-2014, 2014.

586 Wang, Y., Hu, M., Wang, Y., Zheng, J., Shang, D., Yang, Y., Liu, Y., Li, X., Tang, R., Zhu, W., Du, Z., Wu, Y., Guo, S., Wu, Z.,
587 Lou, S., Hallquist, M., and Yu, J. Z.: The formation of nitro-aromatic compounds under high NO_x and anthropogenic VOC
588 conditions in urban Beijing, China, *Atmospheric Chemistry and Physics*, 19, 7649-7665, doi:10.5194/acp-19-7649-2019,
589 2019b.

590 Wu, C. and Yu, J. Z.: Determination of primary combustion source organic carbon-to-elemental carbon (OC_{CaEuro}-/aEuro-EC)
591 ratio using ambient OC and EC measurements: secondary OC-EC correlation minimization method, *Atmos Chem Phys*, 16,
592 5453-5465, 10.5194/acp-16-5453-2016, 2016.

593 Yang, W., Zhang, Y., Wang, X., Li, S., Zhu, M., Yu, Q., Li, G., Huang, Z., Zhang, H., Wu, Z., Song, W., Tan, J., and Shao, M.:
594 Volatile organic compounds at a rural site in Beijing: influence of temporary emission control and wintertime heating,
595 *Atmospheric Chemistry and Physics*, 18, 12663-12682, doi:10.5194/acp-18-12663-2018, 2018.

596 Yao, Z., Shen, X., Ye, Y., Cao, X., Jiang, X., Zhang, Y., and He, K.: On-road emission characteristics of VOCs from diesel
597 trucks in Beijing, China, *Atmospheric Environment*, 103, 87-93, doi:10.1016/j.atmosenv.2014.12.028, 2015.

598 Zhang, Q., Worsnop, D. R., Canagaratna, M. R., and Jimenez, J. L.: Hydrocarbon-like and oxygenated organic aerosols in
599 Pittsburgh: insights into sources and processes of organic aerosols, *Atmos Chem Phys*, 5, 3289-3311, 10.5194/acp-5-3289-
600 2005, 2005.

601 Zhang, Q., Jimenez, J. L., Canagaratna, M. R., Ulbrich, I. M., Ng, N. L., Worsnop, D. R., and Sun, Y.: Understanding
602 atmospheric organic aerosols via factor analysis of aerosol mass spectrometry: a review, *Analytical and Bioanalytical*
603 *Chemistry*, 401, 3045-3067, doi:10.1007/s00216-011-5355-y, 2011.

604 Zhang, Q., Shen, Z., Zhang, L., Zeng, Y., Ning, Z., Zhang, T., Lei, Y., Wang, Q., Li, G., Sun, J., Westerdahl, D., Xu, H., and
605 Cao, J.: Investigation of Primary and Secondary Particulate Brown Carbon in Two Chinese Cities of Xi'an and Hong Kong in
606 Wintertime, *Environmental Science & Technology*, 54, 3803-3813, 10.1021/acs.est.9b05332, 2020.

607 Zhang, Y., Zhang, Q., Cheng, Y., Su, H., Li, H., Li, M., Zhang, X., Ding, A., and He, K.: Amplification of light absorption of
608 black carbon associated with air pollution, *Atmospheric Chemistry and Physics*, 18, 9879-9896, doi:10.5194/acp-18-9879-
609 2018, 2018.

610 Zhao, R., Lee, A. K. Y., Huang, L., Li, X., Yang, F., and Abbatt, J. P. D.: Photochemical processing of aqueous atmospheric
611 brown carbon, *Atmospheric Chemistry and Physics*, 15, 6087-6100, doi:10.5194/acp-15-6087-2015, 2015.

612 Zhou, S., Collier, S., Xu, J., Mei, F., Wang, J., Lee, Y.-N., Sedlacek, A. J., III, Springston, S. R., Sun, Y., and Zhang, Q.:
613 Influences of upwind emission sources and atmospheric processing on aerosol chemistry and properties at a rural location in
614 the Northeastern US, *Journal of Geophysical Research-Atmospheres*, 121, 6049-6065, 10.1002/2015jd024568, 2016.

615
616